**SWIFT-UVOT-CALDB-17-02**
Date Original Submitted: 2015-10-15
Prepared by: A. A. Breeveld
Date Revised: 2022-03-14
Revision #2b
Revised by: A. Breeveld, J. Gelbord*, R. Edelson*,
Sections Changed: most
Comments: updated with better SSS masks in three levels for each filter: Low, Mid, and High


# SWIFT UVOT CALDB RELEASE NOTE

SWIFT-UVOT-CALDB-17: Small Scale Sensitivity

## Summary

This CALDB product provides masks for small regions of low sensitivity in each filter. At present there is no well-defined correction so instead masks are used such that these regions are recognised by a small scale sensitivity (SSS) factor value of -99.9.

## 1 Component Files:

| FILE NAME | VALID DATE | RELEASE DATE | VERSION |
|---|---|---|---|
| swusslsens20041120v001.fits | | | 2 |
| swussmsens20041120v001.fits | | | 2 |
| swusshsens20041120v001.fits | | | 2 |

## 2 Scope of Document:

This document includes a description of the product, expected future updates, warnings for the user, a list of data the product is based on and finally the analysis methods used to create the product.

Other relevant documents are “SWIFT-UVOT-CALDB-15: Sensitivity loss” (uvotcaldb_throughput_06.pdf) and “UVOT Small Scale Sensitivity Regions” (sss_patches.pdf).

## 3 Changes:

This is the second release of a calibration for this product. For this release, three masks (per filter) are supplied with various levels or strengths (Low, Mid, High) for users to choose which is most appropriate for the analysis they are doing.

* J.G. and R.E. gratefully acknowledge support from NASA under the ADAP award 80NSSC17K0126.

### 3.1 CALDB file versions:

**Version 1** swusssens20041120v001.fits
**Version 2** swusslsens20041120v001.fits (**Low**/mild screening)
swussmsens20041120v001.fits (**Mid**/intermediate screening)
swusshsens20041120v001.fits (**High**/aggressive screening)

### 3.2 CALDB content:

In this version the areas of low sensitivity are given the value -99.9, with a value of 1.0 everywhere else. When the SSS file is used with the uvot ftools, the final magnitudes for any sources with centroids falling in the low sensitivity areas are given the value 99 and 'corrected' count rates appear negative.

The three files give the user the choice between Low, Medium or High levels of cleaning. The **Low** level removes the *smallest* number of sources, and is designed to cover all the most strongly affected locations. Each file contains masks for all filters except the grisms and magnifier.

The three different strengths of screening have been defined to allow users to choose the level of data rejection based on their science goals and tolerance of error in the flux measurements. Choosing a more aggressive (**High**) screening will result in rejection of more bad data (dropouts) as well as the loss of more good data, while more conservative (**Low**) screening will result in the rejection of less data (both good and bad). This is the standard trade-off between Type I and Type II errors.

### 3.3 Using CALDB

More information on using the calibration can be found on the UVOT digest page at:
http://swift.gsfc.nasa.gov/analysis/uvot_digest/sss_check.html

## 4 Reason For Update:

The UVOT detector shows small-scale sensitivity inhomogeneities (e.g., Edelson et al., 2015). Sources falling within the small-scale areas of low sensitivity can give count rates of, in the worst case, up to 39% lower than in other areas and thus the photometry is not accurate. This update gives the user better masks and a choice about what level of cleaning is required.

## 5 Expected Updates:

New versions of the calibration may be released as the low sensitivity regions are better defined. In the future we hope to replace the -99.9 factor with real correction factors so that sources falling in the affected areas do not have to be discarded.

## 6 Caveat Emptor:

Some source count rates flagged for discarding may not be significantly affected, either because the effect is weak (say, of order 1–2%) or because the object has low SNR so the flux uncertainty is dominated by other considerations (e.g., photon statistics or background subtraction). Similarly low count rates may still be found in other areas that are not yet identified as low sensitivity regions.

A measured source gets marked for rejection with a mag = 99 value only if the centre of the source extraction region coincides with a low sensitivity region. If some peripheral part of the source region is affected it will not be flagged but could still have a reduced count rate, but the effect is likely to be

very small and other uncertainties will dominate.
The corners and areas within 6 arcsec of the sensor edges have been set to 1.0 so that no checking for low sensitivity regions is available here.

Note, there are as yet no masks for the grisms.

# 7 Data Used:

For making the product:

- Galactic Centre field stars around Sgr A*

For checking the product:

- Data used for throughput trending (uvotcaldb_throughput_06.pdf)
- Field stars from 8 AGN monitoring campaigns

# 8 Description of Analysis: (see also sss_patches.pdf)

In this section the word 'pixel' implies a binned pixel i.e., 1"×1"; most images are binned to this resolution. A 'subpixel' refers to full resolution of 0.5"×0.5".

## 8.1 Regions of low sensitivity: Small Scale Sensitivity

### *8.1.1 NGC 5548*

Intensive sampling (~ 4 months of approximately 2 per day) of the AGN NGC5548 showed some anomalous, abrupt, short-lived dips in count rate that are physically implausible. These dips are seen mainly in the UV filters, with the deepest in UVW2 (by up to 34% in UVW2, 22% in UVM2, 17% in UVW1) (see Figure 1). The dips are weaker in the optical bands. Other stars in the field do not show corresponding dips in their light curves and HST UV data on the same object does not have similar dropouts. Although NGC5548 is a variable source the high volume and density of data allowed the problem to be pinpointed.

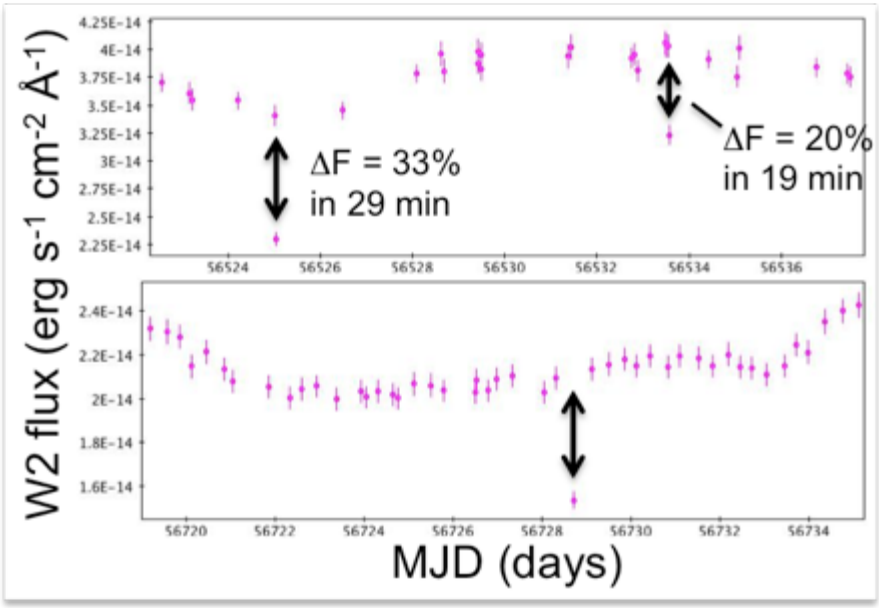


*Figure 1. From Gelbord et al. (2014): UVW2 light curves of NGC 5548 showing dips. Top: two very rapid dips that are difficult to explain physically. Bottom: dip timescale contrasts sharply with other variability in this band.*

The data were checked for any known problems (no image artifacts, elevated backgrounds, tracking errors, etc.).

Gelbord et al. (2014) identified 85 dips by comparing fluxes to neighbouring values in the light curves and found them to be clustered when plotted in raw detector coordinates. The raw coordinates were calculated from the sky coordinates using the telescope pointing parameters. This transformation did not include the distortion map, but even without this correction it was clear that the points lie in certain positions on the detector (see Figure 2). Thus, there appeared to be localised regions of reduced sensitivity.

Edelson et al. (2015) defined boxes containing most of the major clusters of bad points. The boxes covered ~4% of the central 5' x 5' of the UVOT field. The NGC 5548 measurements did not sample the central region uniformly and may have missed some low sensitivity regions (e.g., one of the prominent blemishes marked in Figure 3), implying that the fraction of significantly affected measurements may exceed several percent (see Table 2).

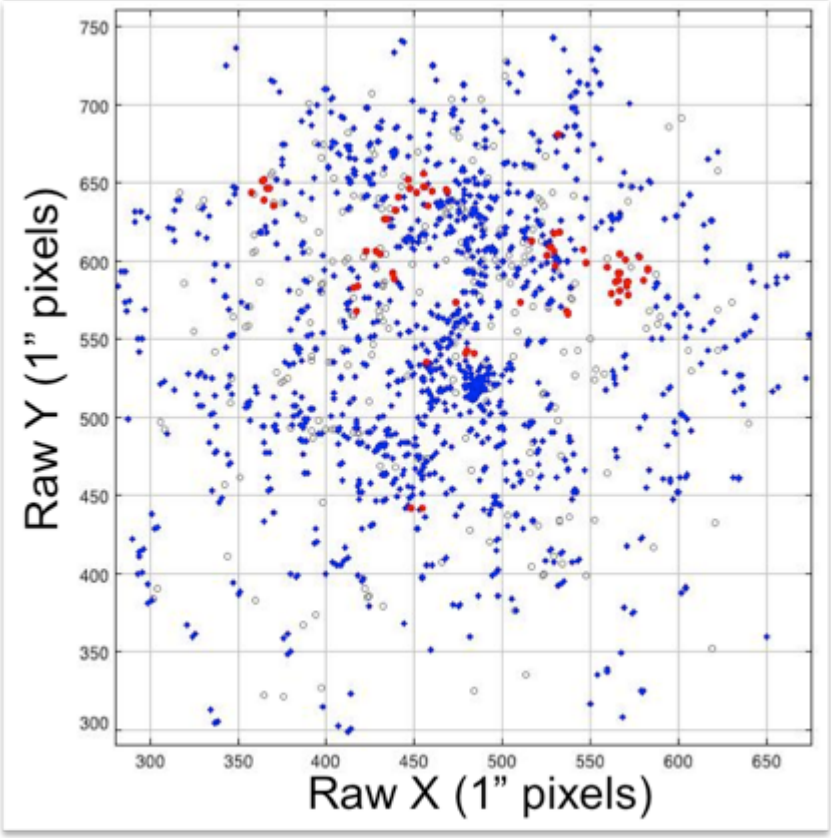


*Figure 2. From Gelbord et al. (2014): Measurements in the detector plane, showing the clustering of verified dips (red circles). Non-dipping flux values are blue diamonds; measurements lacking neighbours within ±2 days are untested (grey open circles).*

### *8.1.2 White Dwarf measurements*

The throughput trending in the UV uses three White Dwarf standards. These have occasionally given implausibly low values, and these outlying values have been removed manually from the data set. The trending observation magnitudes are measured using sky images, however, using the python

routine convertsky2det2raw it was found that in nearly all cases the raw coordinates of the anomalous points lie on the regions of low sensitivity where Gelbord identified dips.

### *8.1.3 LED flat fields and bad pixels*

For calibration in flight, four flood-LEDs are provided. They are located off-axis close to the detector and are positioned so that their emission falls on the side of the filter wheel facing the detector. When the blank filter is put in place, it acts as a defocused "screen" providing the flat field. They are green LEDs but with emission in the UV range (Huckle, 2006). The illumination is fairly even and these images are known as LED flat fields although the illumination is not totally flat. The images are smoothed over the large-scale and summed to make deep images of more than $10^{10}$ counts. These images do show some stable variation in brightness on a subpixel scale and are used annually to identify bad pixels and, by comparing new images with previous ones, any areas where the throughput has declined with time and usage are identified. However, these areas do not correspond with those found by NGC5548 or the white dwarf trending data.

The regions of low sensitivity described above do not coincide with already-identified bad pixels. Bad pixels are identified from the LED flat fields as having a count rate in a CCD pixel more than 3 sigma from the mean (see badpixel document: SWIFT-UVOT-CALDB-01). Looking at a higher resolution scale of subpixels and relaxing the criteria to include bad subpixels with less than 3 sigma from the mean still did not produce any better correlation with the low sensitivity regions.

Directly comparing the LED flat field count rates inside the regions with those outside did not show anything useful. Thus, it appears that the LED flats do not show the same regions of reduced sensitivity. The regions only show up in images taken of the sky.

### *8.1.4 Scattered light background images*

For Breeveld et al. (2010) figure 20 we constructed images of the diffuse scattered sky light by taking many full frame images from the archive and masking out all sources, ghost images and readout streaks to leave just the background light. Unbinned raw images for each filter were summed together using the background level to normalise the values in each subpixel. The resulting images reveal scattered light rings and central enhancement (see also Figure 10). In addition, several small dark patches are seen at identical positions for each filter, but with slightly different patterns for the Optical and UV filters. The number of counts per subpixel in these regions is up to a few percent lower (max 10%) than in the surrounding regions.

The clusters of low sensitivity regions located in the NGC5548 data do coincide with these regions (see Figure 3).

The matching up of the regions shows up best with UVM2 (see Figure 4). In the other filters the scattered light ring partially obscures the low sensitivity regions. In the optical filters there are hints of patches at the same positions, but there are other deeper patches in different positions (see Figure 5). The dropouts in the optical seem to be less of a problem and less deep.

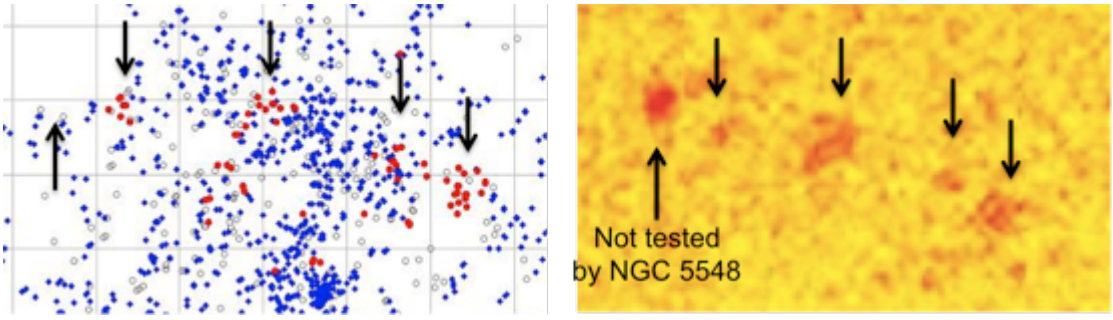


*Figure 3. From Gelbord et al. (2014): A comparison of the distribution of flux outliers to blemishes in a source-subtracted UVM2 background image (Breeveld et al. 2010, MNRAS 406, 1687).*

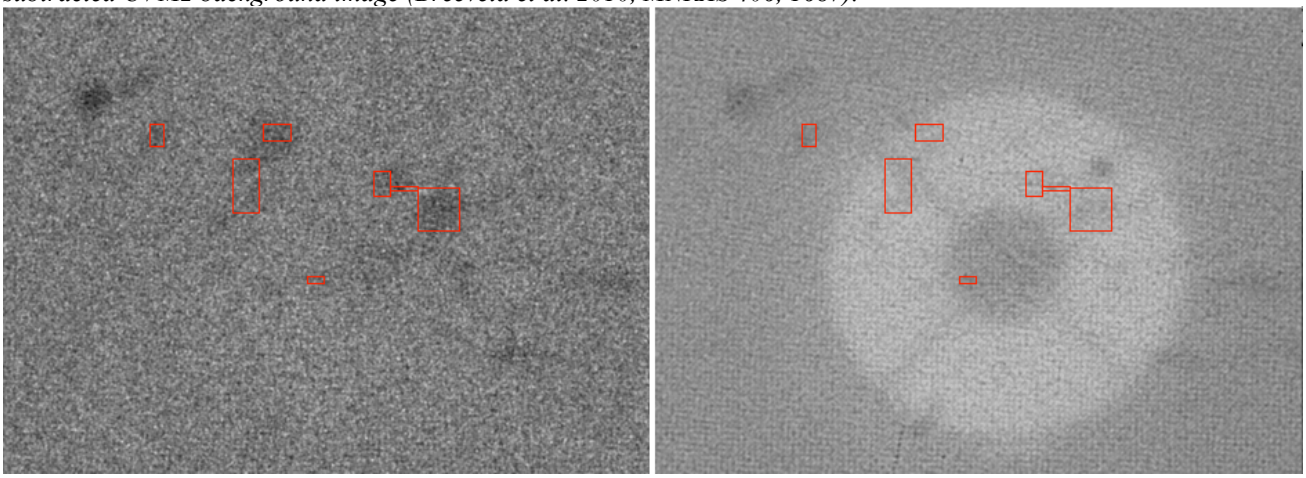

*Figure 4. The central (10') regions of two scattered light images. Left, UVM2 and right, UVW1. The same patches are visible in both, but in UVW1 some of them are partially obscured by the scattered light ring. A set of 7 boxes (defining the low NGC5548 regions) are overplotted on each.*

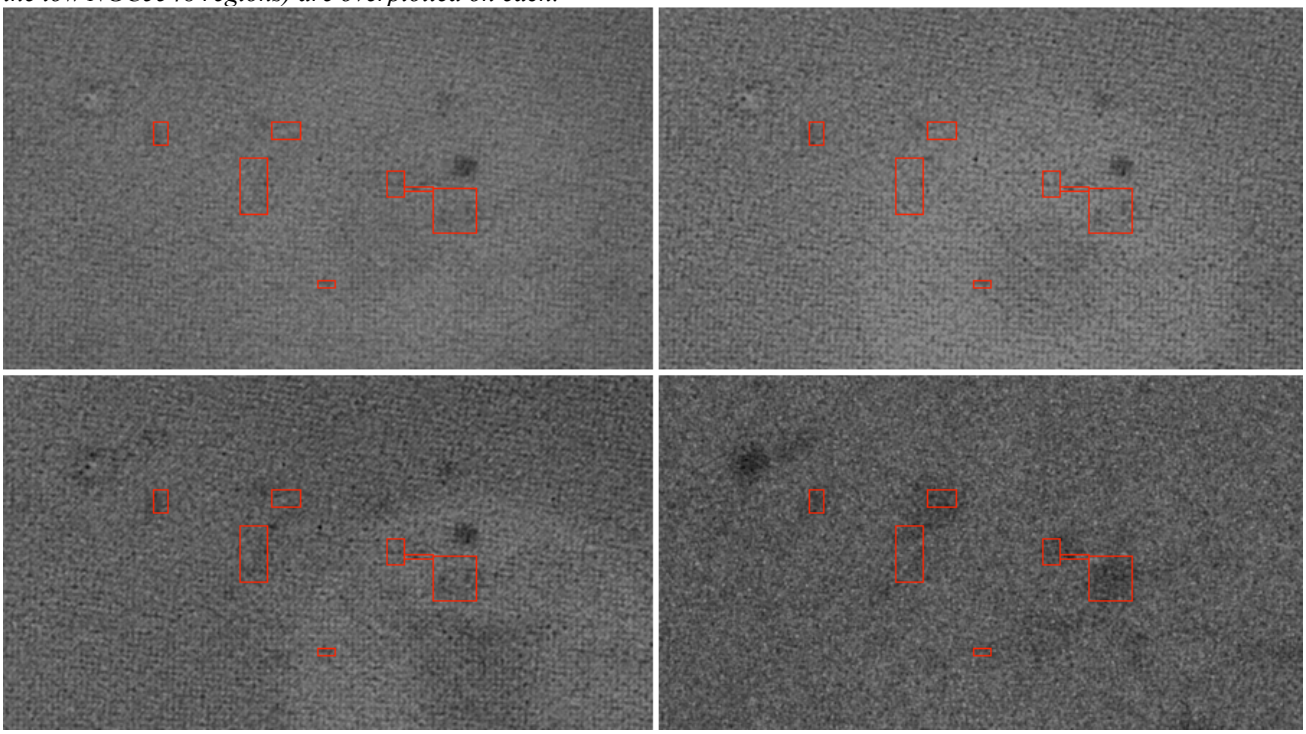

*Figure 5. Showing the difference between the low sensitivity regions in optical filters with those in UVM2. From top left, V,B,U,UVM2.*

Although some of the patches appear to be swamped in the UVW1 and UVW2 filters by scattered

light, dropouts are still measured in these regions. Figure 6 shows the NGC5548 measurements from all the UV filters overlaid on the UVM2 scattered light image. Similarly, there is a dark patch near the bottom in the optical images that does not seem significant in the UV, yet the yellow points marked with an arrow in Figure 6 line up with that patch.

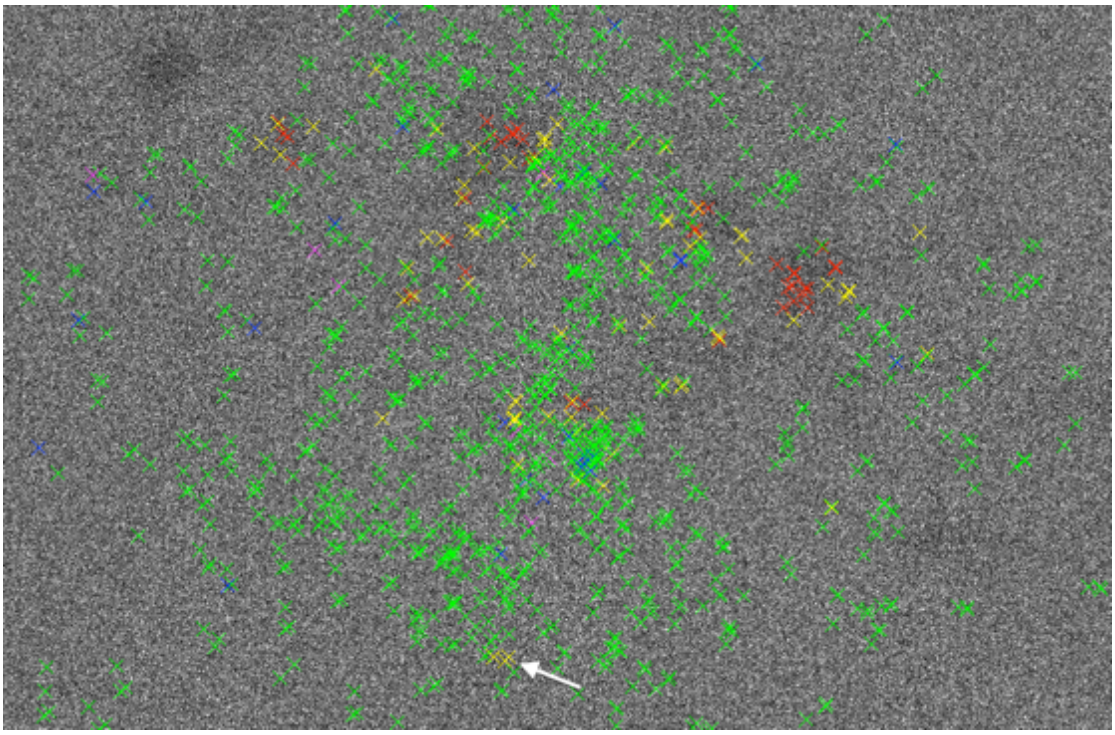

*Figure 6. UVM2 central 10' scattered light image overlaid with NGC5548 measurements. The red crosses are the deepest dropouts with more than 10% reduction, yellow are around 5% reduction, green ok. Blue and purple mark rates that are high compared with the mean. The arrow points to the position of a patch in the optical images that is barely seen in the UV.*

### *8.1.5 Proposed explanation: Dust on photocathode*

It is believed that the regions of low sensitivity are caused by dust or other debris lying loosely on the surface of the photocathode. The collimated light coming from the telescope is scattered by the debris, leaving a shadow, whereas diffuse light from the LED comes from sufficiently random directions not to create the shadow. This also explains why the scattered light seems to be differently affected; the scattered light reaches the detector via a different pathway. The debris material is apparently of a size or nature to absorb the UV light more than optical.

It has to be noted that cleanliness during the manufacture and build of the detector and telescope was treated with the utmost importance, hence the improved throughput in the UV for the UVOT compared with the XMM-OM in which some contamination occurred. Nevertheless, some level of contamination cannot be ruled out.

## 8.2 Creating Small Scale Sensitivity masks for version 2

The procedure for defining and testing the updated SSS masks is described below. An earlier description appears in the appendix of Hernández Santisteban et al. (2020).

### *8.2.1 Galactic Centre Field Star Measurements*

The Galactic Centre is ideally suited to search for regions of low sensitivity because of high stellar density, allowing many points on the detector to be probed in each exposure.

Around 350 sources within 12 arcmin of Sgr A*, were tracked in the U, UVW1, UVM2 and UVW2 filters (Figure 7). Swift has monitored this region of the sky almost daily, providing > 3200 observations between June 2006 and April 2018, yielding 531,132 flux measurements of the tracked stars. There were few observations in the B and V filters.

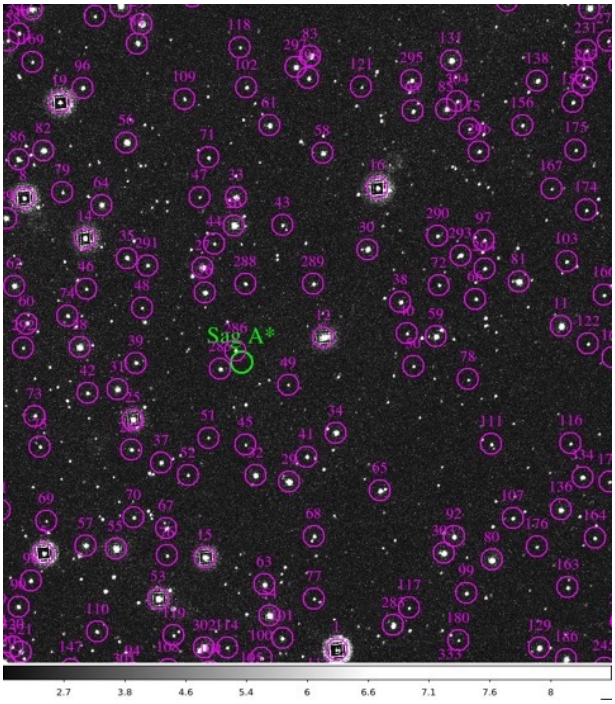


*Figure 7. 14′ × 15′ region around Sgr A*, in U. This region includes ~40% of the tracked stars, which are labelled, enclosed in 15″ circles.*

Light curves were constructed for each source in each filter, then modelled by fitting a polynomial curve within a sliding window. The model flux value at the time of each measurement, ($F_{model}$), is determined by fitting a quadratic to the other light curve points within ±4 months (long enough to span across the annual observing gap when Galactic centre region is Sun constrained). $F_{model}$ values were determined only when the sliding windows encompassed enough data points (at least 9 neighbouring points excluding iteratively-rejected outliers) and included data both before and after the window centre to avoid extrapolated values.

After fitting $F_{model}$, we obtained the deviation:

$$\frac{F_{measured}-F_{model}}{F_{model}} \quad (1)$$

of each measured flux point ($F_{measured}$) (see Figure 8); each point quantifies how much the flux measured at a given location differs from the expected value.

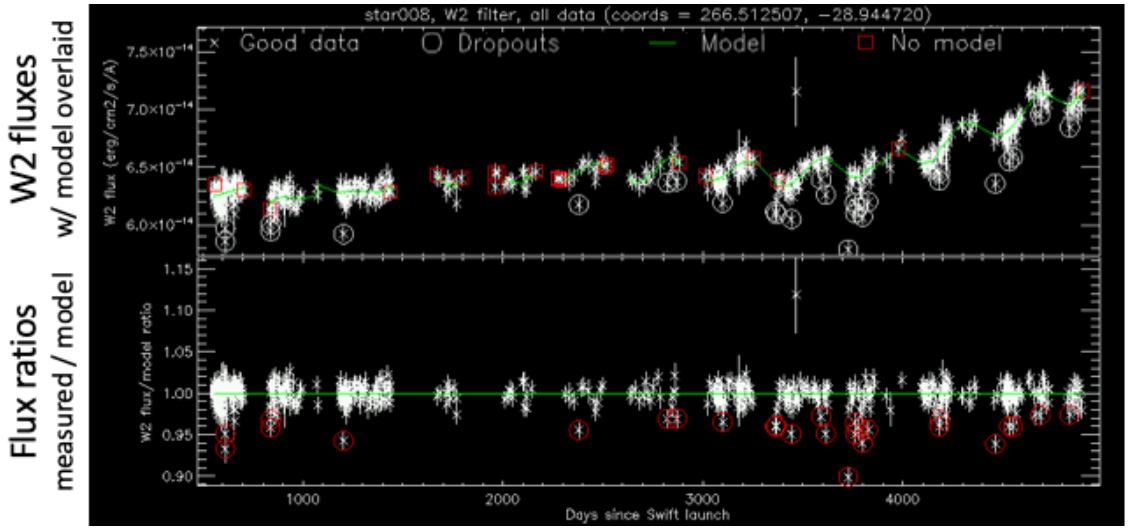


*Figure 8. Example light curves. The fitted model is shown as a green line. Deviant points are marked with circles*

### *8.2.2 Data Screening*

Initial automated checks and manual inspection screened out problematic observations such as those with astrometric errors, distorted PSFs or high backgrounds. Any flux measurements with uncertainties >10% were discarded to avoid low-confidence data when defining stellar light curve models. Light curve models were fitted in all cases with enough remaining data points in the sliding window. Only 52.3% of stellar measurements survived beyond this step; Table 1 (top row) gives the numbers remaining.

Further light curve model screening eliminated light curves with:

i. too few (≤50) data points with fitted $F_{model}$ values.
ii. median error percentage too high (>8% for UVW2 and UVM2 filters or >4% for UVW1 and U).
iii. extreme ratios of mean deviation size to mean measurement error (large ratios indicate inaccurate models with widely scattered measurements suggesting that there was more variability than could be reproduced by the quadratic models, while low ratios suggest that the models are 'too good' and are fitting noise).

The requirement (i) of at least 50 data points eliminates all light curves in B and V.

| | UVW2 | UVM2 | UVW1 | U | Total |
|---|---|---|---|---|---|
| Number of deviation measurements that pass initial data quality tests | 52,874 | 25,774 | 91,151 | 107,850 | 277,649 |
| Number and % remaining after applying light curve model screening | 45,724 (86.5%) | 21,701 (84.2%) | 49,172 (53.9%) | 92,707 (86.0%) | 209,304 (75.4%) |
| High SNR measurements used to define heat maps | 30,886 (58.3%) | 14,663 (55.6%) | 31,919 (35.0%) | 59,250 (54.9%) | 136,718 (49.2%) |

*Table 1. Number of measurements per filter remaining after initial quality checks, light-curve-model screening and SNR cuts (see next section). No light curve in B or V filter had sufficient data points.*

### *8.2.3 Heat map definition*

The fractional deviation from the light curve model was evaluated for each measurement. The

position of the measurement was then mapped onto an image of the detector in raw coordinates to build up a map of fractional deviations. Binning 2×2 is adopted throughout, hence each image is an array of 1024 × 1024 one-arcsec pixels, but despite the binning, measurements are still sparse across the detector plane. A SNR cut was applied to eliminate the lower-quality deviation measurements (eliminating those with flux measurement errors >5.5% in UVW2 and UVM2, >3.0% in UVW1, >2.5% in U), resulting in 15k-59k values per filter spread across the $10^6$ pixels in the image.

'Heat maps' for each filter were generated by smoothing over the mapped fractional deviations. Gaussian smoothing, weighted by distance, was used to assign an average value to each pixel. Smoothing was needed to both fill gaps and ensure pixel values have reasonable statistics.

Figure 9 shows the resulting maps, smoothed with a kernel of 5". The dark patches indicate strong negative deviations where the measured fluxes are systematically low. These regions show a similar pattern, filter-to-filter. The light areas indicate positive deviations where fluxes are systematically high and these patterns differ between filters. There are insufficient data to make maps in B, V. The corners and areas within 6 pixels (6") of the edges have been masked out because vignetting and edge effects make it difficult to identify low sensitivity regions here.

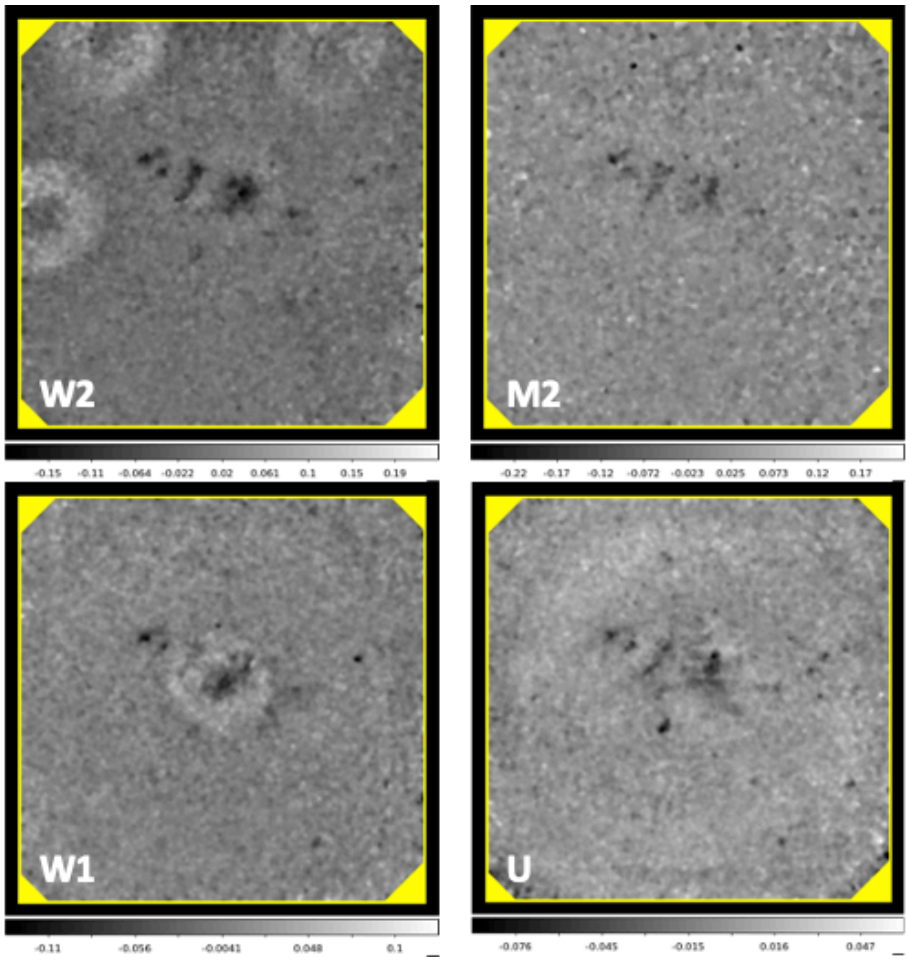


*Figure 9. Heat maps made using a smoothing kernel of 5". Strong dropout regions appear black. The number of measurements used to generate these maps are given in Table 1. Note: grey scale for each map is min-max; ranges are actually much smaller in U and UVW1. The images here are the full field of 17'x17'.*

### *8.2.3.1 Comparison with source-subtracted backgrounds.*

As expected from Section 8.1.4 there is close agreement between the low sensitivity regions illustrated in the heat maps and those seen in the scattered light background images (Figure 10). Light areas in the form of rings are seen in both, and the dark regions are distributed similarly but are more well-defined in the heat maps. The consistency implies that the low sensitivity regions have been present in the UVOT since early in the mission because figure 20 in Breeveld et al. (2010) was generated in the first 5 years.

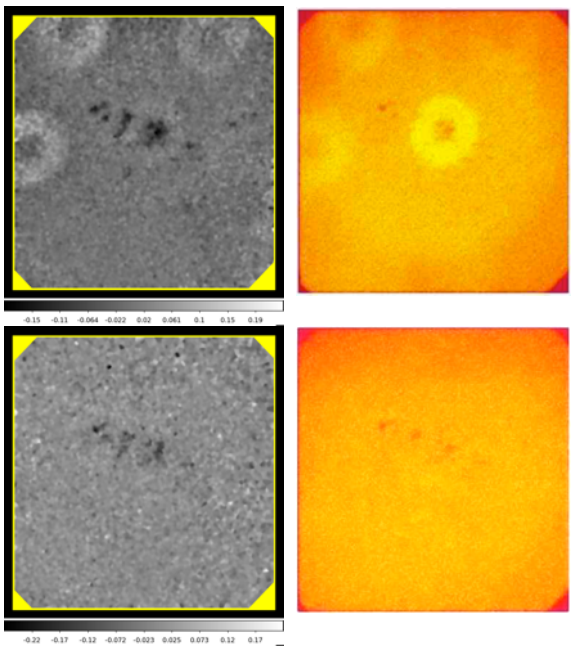

*Figure 10. Left: UVW2 and UVM2 heat maps of the full frame (17'x17') using smoothing kernel of 5". Right: the corresponding scattered light images from Breeveld et al. 2010.*

### *8.2.3.2 Choosing smoothing parameters and summing heat maps*

Each pixel in the heat map is an average of the surrounding fractional deviations, weighted by distance and smoothed. The smoothing length needs to be large enough to provide reasonable statistics for defining each point, but small enough so that detail in the map is not lost. Similarly, heat maps defined for each UV filter individually will have poorer statistics than if the three UV maps are combined; combined maps benefit from a denser sampling of the detector plane but may lose information that is distinct to a particular filter.

To investigate both these issues, heat maps were tested with an independent set of data. For the map definition we had used Sgr A* field star data; for the evaluation, the field stars from 8 AGN monitoring campaigns for which observations were made at least once per day and were within the central 4.5' x 4.5' region of the detector (approx$10^3$ data points per filter). We obtained light curves and deviations from the independent sample following the same procedure and applying the same screening as for the Sgr A* data. We then evaluated the correlation between the flux deviations and the heat map values as a function of smoothing kernel (Figure 11) and used the correlation coefficient to identify the best maps.

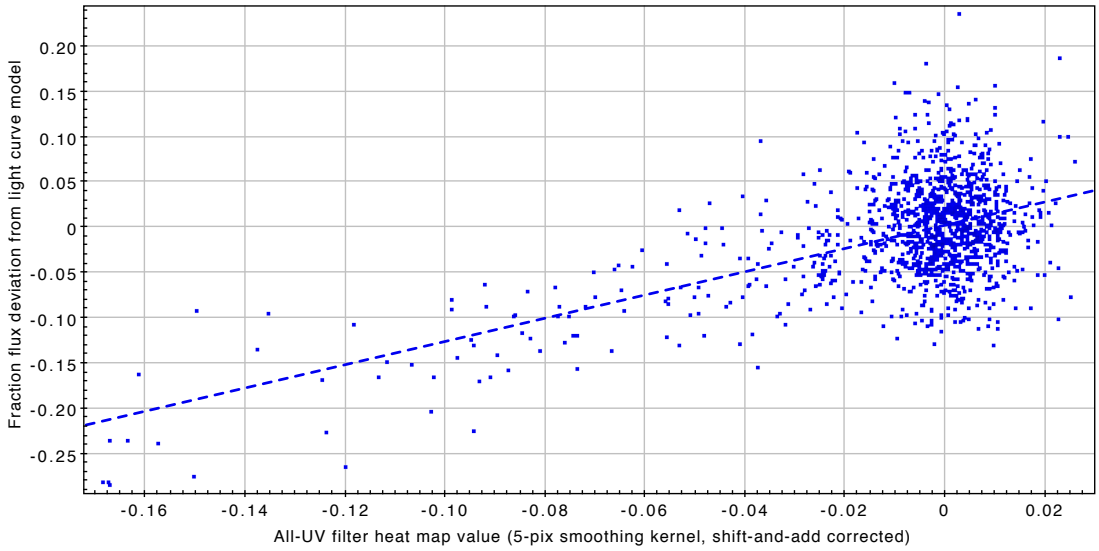


*Figure 11. Correlation between flux deviations and the value in the heat map at that source position for uvm2. The dashed line is a least-squares fit to the data.*

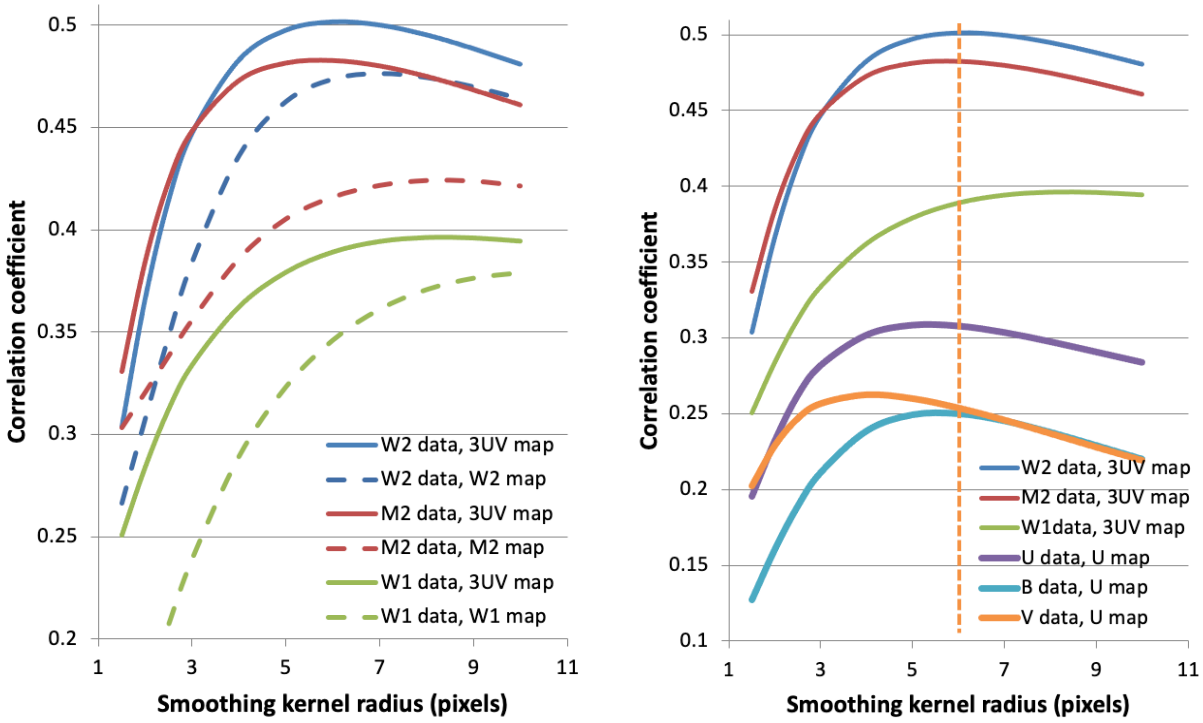


*Figure 12. Evaluating the impact of (left) summing heat maps for UV data, and (right) the effect of the smoothing kernel.*

Figure 12 (left) shows correlations between the measured flux deviations in the test set and the heat map values. Combining all three UV maps leads to a stronger correlation than for the UV maps individually. V and B correlations were found to be stronger when the U map is used for these filters than the UV maps (V and B heat maps could not be made because of lack of data, see section 8.2.2). Figure 12 (right) shows how the strength of the correlation varies with kernel radius. With the three UV maps combined, and using U for all the optical filters, a kernel radius of 5 pixels (5") was chosen for consistency across all the maps.

### *8.2.4 Defining masks from the heat maps*

The SSS masks need to identify regions of the detector where the sensitivity is below a certain threshold in the heat maps. The choice of threshold determines the number and size of the low sensitivity regions masked. Three different thresholds have been defined for low (conservative), mid (intermediate) or high (aggressive) screening to allow users to choose the level of dropout rejection based on their science goals and tolerance of error in the flux measurements. Choosing a more aggressive screening will result in the rejection of more bad data (dropouts) as well as the loss of more good data, while more conservative screening will result in the rejection of less data (both good and bad). This is the standard trade-off between false positive and false negative errors.

Figure 13 shows the correlation between flux deviations and the heat map values. The vertical dashed line indicates a possible threshold such that points to the left of the line would be masked out. It is clear that even if the dashed line were set at a very low heat map value, some points with positive flux deviations (i.e., points that lie above the light-curve model) would still be masked out. To define the heat map thresholds, we use the fraction of test sample measurements to the left of the threshold that will be flagged despite having fluxes that are high relative to the light curve model: for the Low threshold, 10% of the masked points have positive deviations while for the High threshold this number is 25%, with Mid at 20%.

For each filter, different thresholds are required to achieve these criteria. This is partly because the straight line fit between flux deviations and heat map values (as in Figure 11 and Figure 13) becomes shallower for the optical filters where the low sensitivity regions do not have such a severe effect.

In the CALDB files the keyword MSK_KERN gives the kernel smoothing radius, and MSKTHRSH gives the threshold for the heat map below which the masked areas are defined. Table 2 shows how much of the detector area is affected by the different mask levels for the different filters.

Figure 14 illustrates the effect of the High cut off threshold on the distribution of flux deviation measurements. The masking removes the tail of low values.

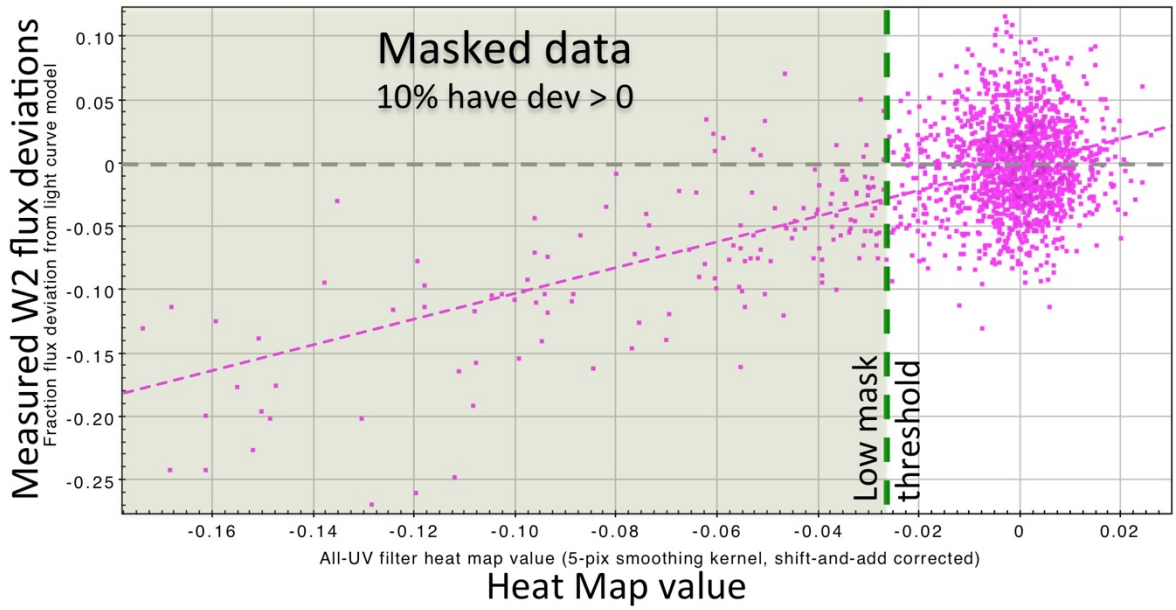


*Figure 13. Flux deviations plotted against the heat map values for uvw2. The vertical dashed green line illustrates the effect of choosing a threshold on the number and deviation of the eliminated points. The fraction of points above the horizonal dashed line and to the left of the green dashed line are used to define where the threshold should go.*

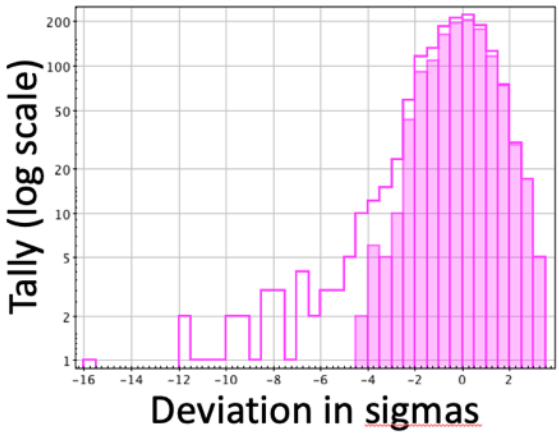


*Figure 14. The effect on the distribution of flux measurements of using the High (aggressive) mask. The final distribution (solid pink) is more symmetric than the original distribution (pink outline).*

| Filter | Low (conservative) | High (aggressive) |
|---|---|---|
| **UVW2** | 8.2% | 14.9% |
| **UVM2** | 9.6% | 14.7% |
| **UVW1** | 5.5% | 13.3% |
| **U** | 4.9% | 10.0% |
| **B** | 2.1% | 4.5% |
| **V** | 1.7% | 4.2% |

*Table 2. The percentage of the middle 5'x5' part of the field of view identified as regions of low sensitivity for the Low and High masks.*

## 8.3 Evaluating the masks using standard stars

Since launch a set of standard stars has been used to monitor the detector throughput. As mentioned in 8.1.2 some of the data points were anomalously low, and these have mostly been confirmed as lying on the low sensitivity regions. These standard star data have been used to evaluate the proportion of data points correctly flagged by the masks, and the proportion of apparently 'good' points also flagged. The advantage of using the standard star data is that there should be no or very little intrinsic variation so the actual deviation of any data point from the mean can be used to assess whether the point is anomalous.

Starting from the null hypothesis that a 'source centroid falling in a masked low sensitivity region should be rejected because its flux is significantly affected by detector inhomogeneities', we define a false positive (Type I error) such that a source is flagged when it is only marginally (not significantly) affected or not affected; a false negative (Type II error) is when a source is *not* flagged despite being significantly affected.

Using these standard star data, we addressed the following questions for each filter and each of the three levels of masking (low, mid and high), to assess the rate of false positives and false negatives:

- How many confirmed dropouts are identified in the data?
- How many of these are successfully flagged by the mask?
- What is the rate of false positives? In other words, how many seemingly-good measurements are flagged as dropouts by the SSS file?
- What is the rate of false negatives? In other words, how many dropouts are missed?

The ftool uvotmaghist was run on all the standard star exposures using each of the SSS CALDB files in turn.

During the first exposure the pointing can still be changing, and the "shift and add" procedure chooses the very first frame, shifting all the other frames to line up with this one, meaning that the raw coordinates can be wrong. This can lead to incorrect flagging either way. Dropouts that were missed or incorrectly flagged were checked by comparing the time of the exposure with the pre-planned science target list (PPST) to see if the exposure was the first after a slew. These exposures (8 in all) were then removed from the input lists. In normal data processing the user will not know whether exposures were the first since a slew, but there are imminent updates to the UVOT software to take this issue into account when applying the SSS calibration.

We defined 'dropouts' as those measurements where the count rate was below the mean for that object by more than 3 standard deviations, and also deviant by more than 3 times the error for that measurement. Data points that do not satisfy this definition for 'dropout' are described as 'good', although note that these will include points for which the reduced sensitivity regions have a weak influence. Table 3 gives the numbers of dropouts correctly identified by the previously released SSS mask and the new sets of masks, the number missed corresponding to the false negative count. Table 4 shows the number of false positives; we refer to these as spuriously flagged even though some are likely to be affected by reduced sensitivity (see section 8.4).

| **Filter** | Total dropouts | Number correctly identified | | | | Percentage correctly identified (%) | | | |
|---|---|---|---|---|---|---|---|---|---|
| | | Previous release | Current release | | | Previous release | Current release | | |
| | | | low | mid | high | | low | mid | high |
| **V** | 6 | 2 | 4 | 4 | 6 | 33 | 67 | 67 | 100 |
| **B** | 12 | 1 | 9 | 9 | 11 | 8 | 75 | 75 | 92 |
| **U** | 11 | 1 | 9 | 10 | 10 | 9 | 82 | 91 | 91 |
| **UVW1** | 24 | 13 | 24 | 24 | 24 | 54 | 100 | 100 | 100 |
| **UVM2** | 19 | 11 | 17 | 18 | 18 | 58 | 89 | 95 | 95 |
| **UVW2** | 37 | 17 | 30 | 33 | 34 | 46 | 81 | 89 | 92 |
| **White** | 22 | 4 | 18 | 19 | 20 | 18 | 82 | 86 | 91 |

*Table 3. The number of dropouts detected in the standard star exposures. Column 1: total dropouts identified by having count rates more than 3sd below the mean. Columns2-5: total dropouts correctly identified and flagged by the SSS masks. Columns 6-9: same as cols 2-5 but converted to percentages. The number of false negatives is the inverse of these numbers.*

| **Filter** | Total good | Number of false positives | | | | Percentage false positives (%) | | | |
|---|---|---|---|---|---|---|---|---|---|
| | data points | Previous release | Current release | | | Previous release | Current release | | |
| | | | low | mid | high | | low | mid | high |
| **V** | 1217 | 0 | 29 | 65 | 91 | 0 | 2 | 5 | 7 |
| **B** | 1046 | 1 | 19 | 62 | 76 | 0 | 2 | 6 | 7 |
| **U** | 932 | 0 | 66 | 170 | 232 | 0 | 7 | 18 | 25 |
| **UVW1** | 432 | 7 | 44 | 85 | 128 | 2 | 10 | 20 | 30 |
| **UVM2** | 345 | 10 | 38 | 63 | 69 | 3 | 11 | 18 | 20 |
| **UVW2** | 354 | 7 | 29 | 51 | 68 | 2 | 8 | 14 | 19 |
| **White** | 562 | 0 | 28 | 106 | 144 | 0 | 5 | 19 | 26 |

*Table 4. The number of data points in the trending data exposures spuriously flagged by the masks (false positives). Column 1: total good data points (within 3sd of the mean). Columns2-5: total good points spuriously flagged as dropouts by the SSS masks. Columns 6-9: same as cols 2-5 but converted to percentages.*

Figure 15 and Figure 16 show an example of the standard star analysis for the UVW2 filter. In Figure 15 the previous SSS file was used, and the Low mask. In Figure 16 the Mid SSS and High SSS masks were used. The data for each target source appear as clumps or lines with a solid green line indicating the mean count rate for that source. Dashed green lines outline where the ±3x standard deviation range lies for each target source. Means and standard deviations were calculated using only data remaining after using the High mask to remove any outliers. Blue circles show any points ("measured dropouts") lying outside the ±3sd ranges indicated by the green dashed lines. Red points are those identified as being on low sensitivity regions by the different masks. In the perfect case all the blue circles would be accompanied by red crosses, and no red crosses would be within the green dashed line boundaries. Red crosses within the ±3sd ranges indicated by the green dashed lines represent the false positives, while blue circles unaccompanied by a red cross are false negatives.

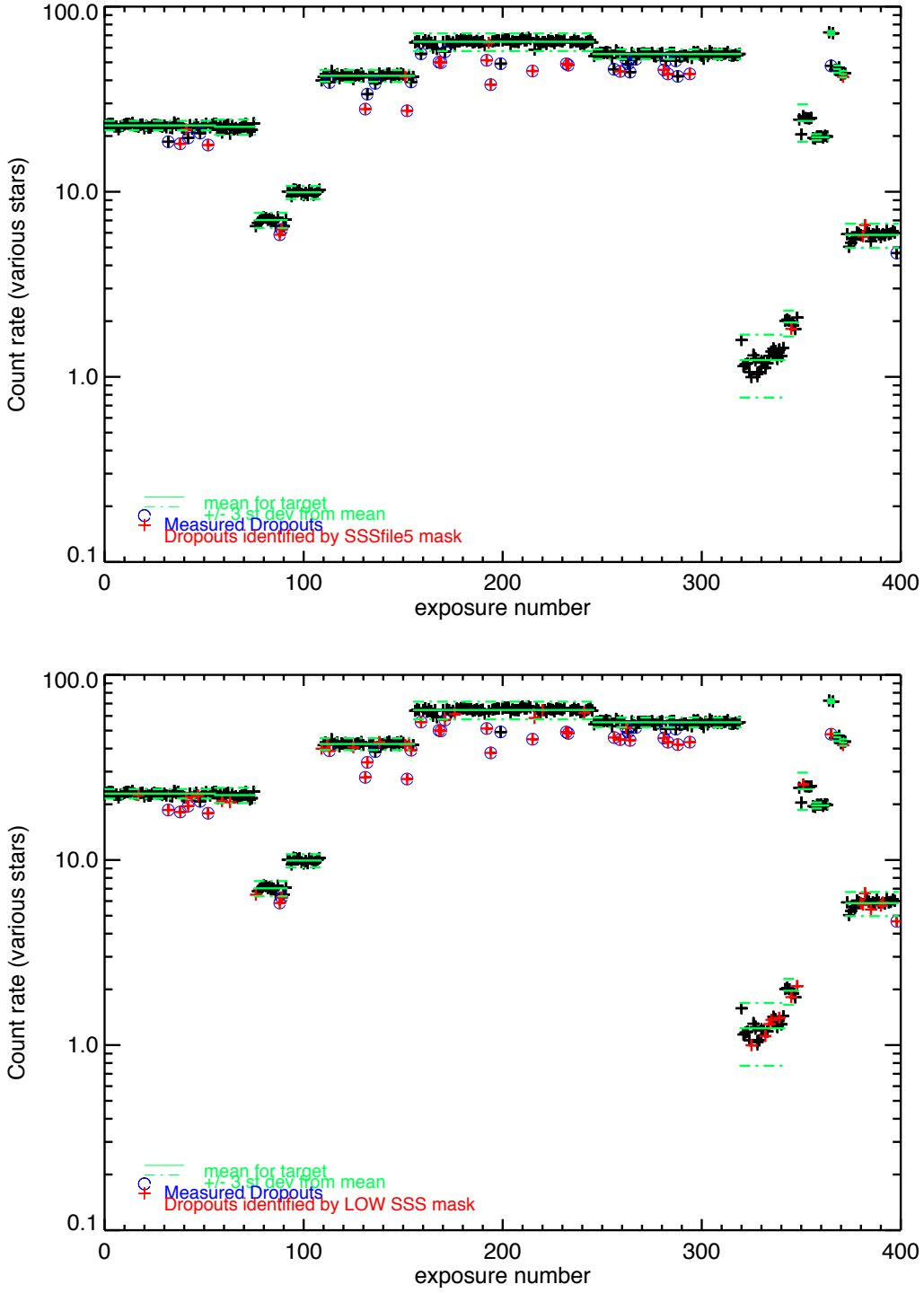


*Figure 15. Trending source data for uvw2 with old mask (top) and new Low mask (bottom). Green lines: means and ±3 standard deviations for each source; Blue circles: measured dropouts; Red crosses: source on a low sensitivity region found by **top**: SSSfile5, **bottom**: Low mask for uvw2 from swusslsens20041120v001.fits. Red crosses within the ±3sd ranges indicated by the green dashed lines represent the false positives, while blue circles unaccompanied by a red cross are false negatives.*

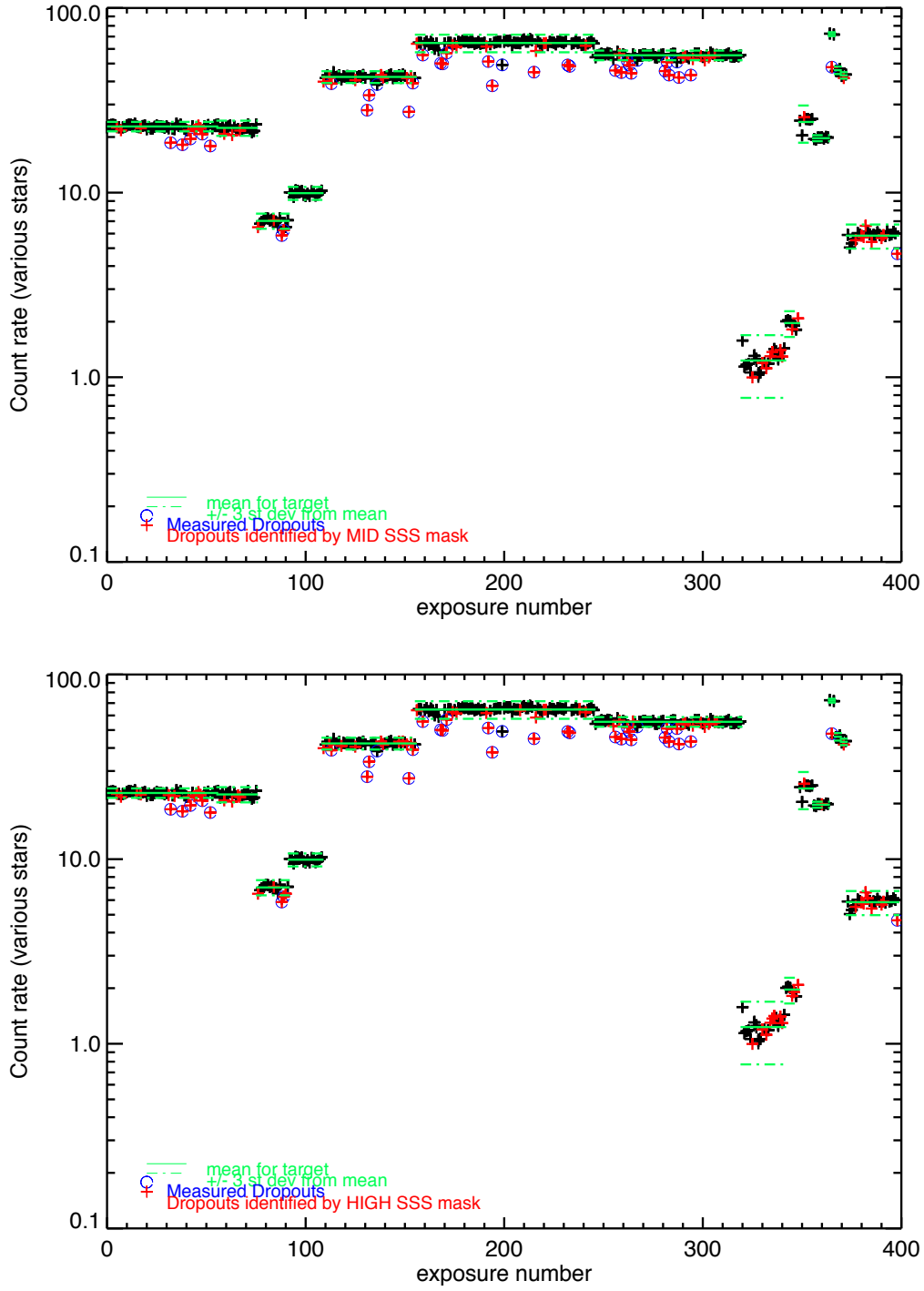


*Figure 16. Trending source data for uvw2 with Mid (top) and High (bottom) masks. Green lines: means and 3 standard deviations for each source; Blue circles: measured dropouts; Red crosses: source on a low sensitivity region found by* ***top****: Mid mask swussmsens20041120v001.fits,* ***bottom****: High mask for uvw2 from swusshsens20041120v001.fits. Red crosses within the ±3sd ranges indicated by the green dashed lines represent the false positives, while blue circles unaccompanied by a red cross are false negatives.*

Some dropouts were low for a different reason such as the data in the image being incomplete (indicated by header keywords such as STALLOSS, BLOCLOSS or TOSSLOSS); the source being on the edge of the image, or the source image being streaked. These were pruned out manually from

the dataset.

Points to note:

- Using a limit of three standard deviations below the mean might be over generous: some of the points within the +/– 3sd range might still be on low sensitivity regions, even though the range has been set by the most stringent dropout removal (aggressive map).
- There are more SSS dropouts in the UV, as expected because the low sensitivity regions are deeper as you move further into the UV, but most of them are flagged, even with the Low map: 81-100%.
- In the UV, using the Low mask catches at least 8 out of 10 dropouts, and flags just 1 in 10 seemingly-good measurements.
- In the UV, the High mask does not catch many more, but might flag 3 in 10 good data points.
- The optical maps do not work so well because the low sensitivity regions are not as deep (the slope in the equivalent plot shown in Figure 13 is much shallower). The masks flag only 67-82%, but also erroneously flag fewer potentially good points.

If only part of a source region lies on a low sensitivity region, then those pixels are necessarily towards the edges of a low sensitivity patch, where the flux suppression is likely no more than a few percent. Given that the UVOT PSF FWHM is of ~2.5", pixels at the edges of the 5" region file will make only a small contribution to the overall source flux. If these pixels are suppressed by a few percent, then the impact on the integrated flux of the source should be much smaller than the measurement uncertainty. For this reason, only sources whose centroid lies on a low sensitivity region are flagged.

### 8.4 Results of using the new masks

An example of the use of the SSS masks for science is shown in Figure 17 where the High/aggressive masks were used to screen light curve data for multi-filter monitoring (an expanded sample that include the eight AGN fields used in section 8.2.3.2 and subsequent sections). In this case of high precision monitoring, aggressive masking was chosen because contamination of the light curve by just a few bad points would be more problematic than the loss of a relatively larger number of good points. That is, in this case false positives are more acceptable than false negatives. In other cases (e.g. discovery surveys), the opposite trade-off is more desirable.

To compare the effects of the different sets of masks, we applied them to a set of 9300 measurements of background stars in fields around AGN with intensive multi-filter monitoring. For each measurement the percentage deviation (Equation 1) from the stellar light curve is determined. In going from Low to Mid to High masks, progressively more data are marked for removal. In Table 5 we present the mean deviations in each filter for four subsets of measurements: those flagged by the Low mask, the additional points flagged by Mid mask but not the Low one, the ones flagged by the High mask but not the Mid, and the points not flagged by any masks. Also provided are the lowest deviations flagged by the Low mask in each filter, which reveals the most extreme cases: up to 10% in V and approaching 40% in W2. It also shows that the additional points flagged by progressively more stringent masks are, on average, still affected by the low sensitivity regions, albeit at a lower level (the mean fluxes are reduced by 0.6-1.8% in the case of points caught by the Mid mask but not the Low, 0.4-0.9% for points flagged by the High but not the Mid mask). Note that other flux uncertainties (such as photon counting statistics or background subtraction) will in many cases be higher than the deviations caught by the Mid or High masks.

## 8.5 Changes with time

In Section 8.2.3.1 we suggested that the low sensitivity areas had not changed since early in the mission. To test this further the Sgr A* data used to prepare the heat maps, was divided into two sets based on time: "early" consists of all data taken from launch to 2012, while "late" includes all data taken from the start of 2013 through to April 2018. Heat maps were prepared for each of these data subsets and compared by ratio. Note that the heat map values are based upon the deviations of measurements from the fitted light curves of each star, so the values are centred about zero and are typically +/- a few percent. Consequently, the ratio values are defined as [(late+1)/(early+1)]-1.0, evaluated pixel-by-pixel.

Figure 18 and Figure 19 show that there is little difference between the early and late heat maps, in spatial distribution and in amplitude of the low sensitivity regions.

| Filter | Low mask | | Mid, not Low | High, not Mid | Never masked | Number of measurements |
|---|---|---|---|---|---|---|
| | avg % | max % | avg % | avg % | avg % | |
| V | -2.0% | -10% | -1.2% | -0.9% | +0.06% | 2321 |
| B | -3.5% | -12% | -1.6% | -0.5% | -0.10% | 2438 |
| U | -4.5% | -16% | -1.4% | -0.6% | -0.31% | 1695 |
| UVW1 | -3.4% | -16% | -0.6% | -0.4% | -0.12% | 882 |
| UVM2 | -5.3% | -28% | -1.8% | -0.6% | +0.15% | 804 |
| UVW2 | -5.0% | -39% | -1.1% | -0.6% | +0.03% | 1178 |

*Table 5. The average percentage flux deviation from the light curve model for measurements flagged by the Low mask (col. 2), the maximum deviation seen in measurements flagged by the Low mask (col. 3)(N.B. the Low mask is designed to cover all the most strongly affected locations); the average deviation for the additional points flagged by Mid mask but not the Low one (col. 4); the average deviation for the ones flagged by the High mask but not the Mid (col. 5); and the average deviation of points not flagged by any masks (col.6). Column 7 gives the total number of measurements included in the test.*

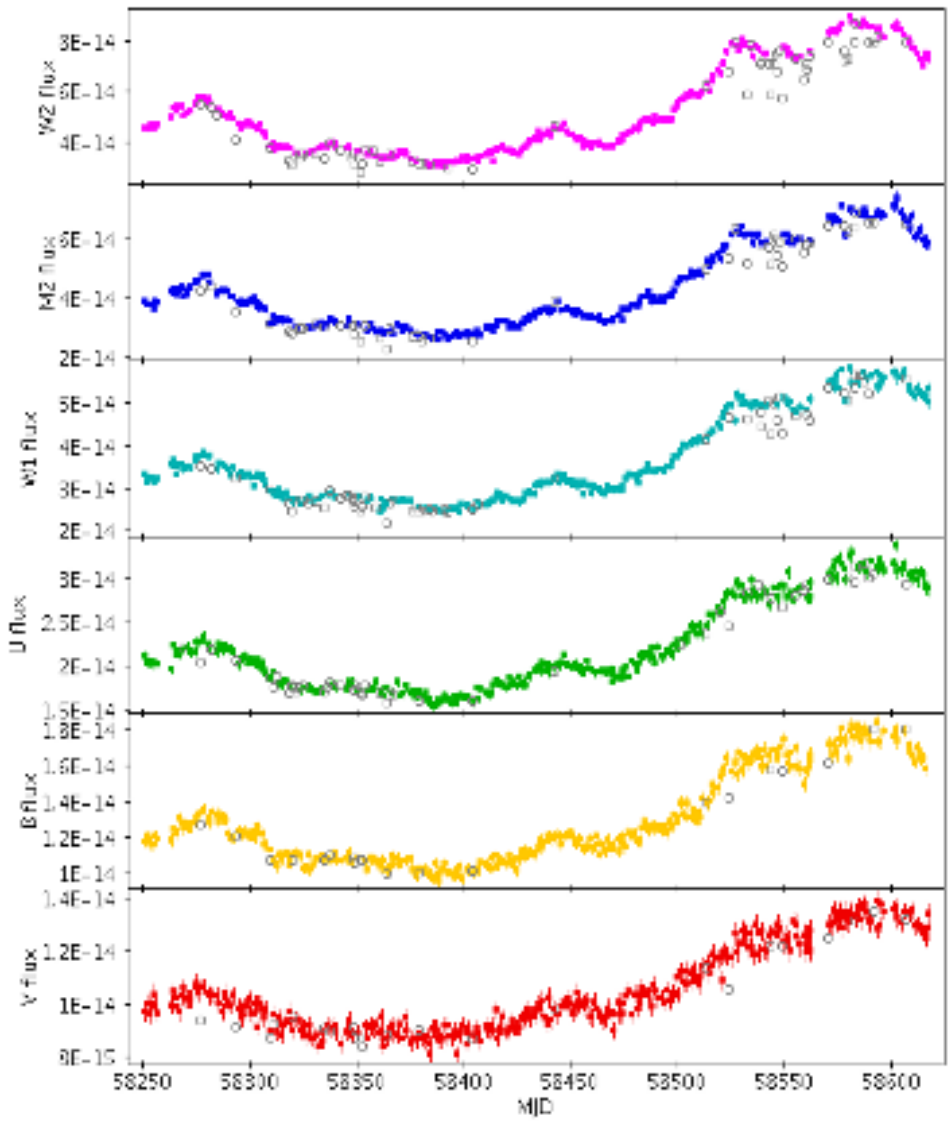


*Figure 17. One-year light curves of Fairall 9 (Hernández Santisteban et al. 2020). Open grey circles are points eliminated by High (aggressive) mask; filled colour points survive screening. Note that the masked points sometimes occur in bunches, rather than being distributed randomly throughout the light curves. This is because where a target falls on the detector plane tends to be correlated from day to day, evolving gradually through the year as the spacecraft roll angle changes. Consequently, during a shorter monitoring campaign (of a few weeks to a month or so) an unlucky target might be affected by the SSS regions with a significantly higher frequency than average.*

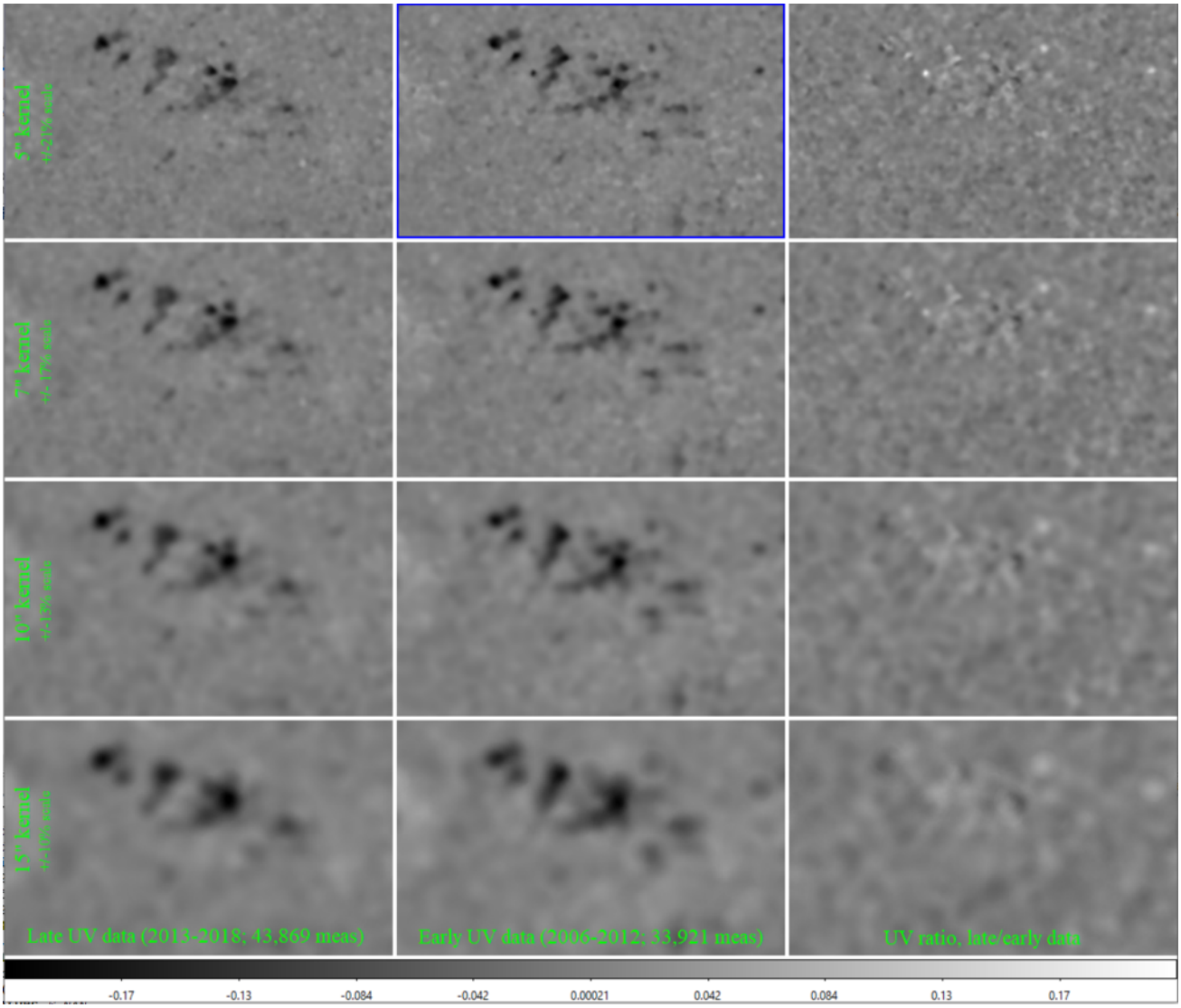


*Figure 18. Comparing UV heat maps produced using data before and after 2012. Left column: later data heat maps with four different smoothing kernels; middle column: earlier data with corresponding smoothing; right column: heat map ratios. Each image covers the central 12' region.*

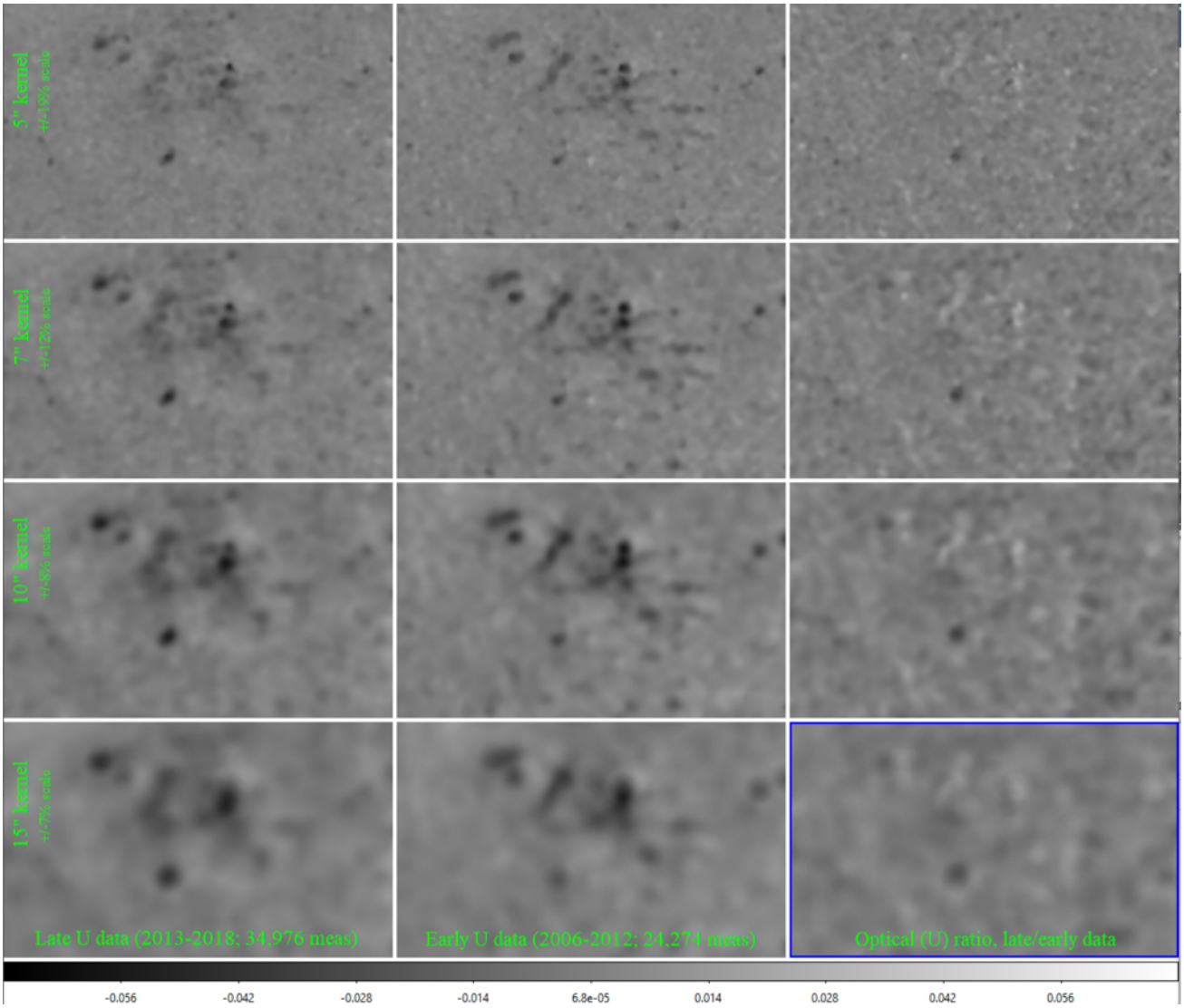


*Figure 19. The equivalent images to Figure 18 but using U data.*

## References

Breeveld A. A. et al. (2010). Further calibration of the Swift ultraviolet/optical telescope. *MNRAS* **406**, 1686-1700

Edelson R. et al. (2015). Space Telescope and Optical Reverberation Mapping Project. II. Swift and HST Reverberation Mapping of the Accretion Disk of NGC 5548. *ApJ* **806**, 129

Gelbord J. et al. (2014). Exploring Multiwavelength AGN Variability with Swift Archival Data, *Proceedings of Swift: 10 Years of Discovery (SWIFT 10)*, held 2-5 December 2014 at La Sapienza University, Rome, Italy. Online at http://pos.sissa.it/archive/conferences/233/137/SWIFT%2010_137.pdf. [Accessed: Nov 22nd 2021]

Hernández Santisteban et al. (2020). Intensive disc-reverberation mapping of Fairall 9: first year of Swift and LCO monitoring. *MNRAS* **498**, 5399

Huckle H. (2006). Swift UVOT users guide: SWIFT-UVOT-302-R04. Online at https://www.mssl.ucl.ac.uk/www_astro/uvot/uvot_instrument/instrument.html [Accessed: Feb 9th 2022]